

Concomitant appearance of conductivity and superconductivity in (111) LaAlO₃/SrTiO₃ interface with metal capping

R. S. Bisht¹, M. Mograbi¹, P. K. Rout¹, G. Tuvia¹, Y. Dagan^{1,*}, Hyeok Yoon^{2,3}, A. G. Swartz^{2,3}, H. Y. Hwang^{2,3}, L. L. Li⁴, and R. Pentcheva⁴

¹School of Physics and Astronomy, Tel-Aviv University, Tel Aviv, 6997801, Israel

²Department of Applied Physics, Geballe Laboratory for Advanced Materials, Stanford University, 476 Lomita Mall, Stanford, CA 94305, USA

³Stanford Institute for Materials and Energy Sciences, SLAC National Accelerator Laboratory, Menlo Park, California 94025, USA

⁴Department of Physics and Center for Nanointegration Duisburg-Essen (CENIDE), University of Duisburg-Essen, Lotharstr. 1, D-47057 Duisburg, Germany

*yodagan@tauex.tau.ac.il

ABSTRACT

In polar-oxide interfaces, a certain number of monolayers (ML) is needed for conductivity to appear. This threshold for conductivity is explained by accumulating sufficient electric potential to initiate charge transfer to the interface. Here we study experimentally and theoretically the (111) SrTiO₃/LaAlO₃ interface where a critical thickness, t_c , of nine epitaxial LaAlO₃ ML is required to turn the interface from insulating to conducting and even superconducting. We show that t_c decreases to 3ML when depositing a cobalt over-layer (capping) and 6ML for platinum capping. The latter result contrasts with the (100) interface, where platinum capping increases t_c beyond the bare interface. The observed threshold for conductivity for the bare and the metal-capped interfaces is confirmed by our density functional theory calculations. Interestingly, for (111) SrTiO₃/LaAlO₃/Metal interfaces, conductivity appears concomitantly with superconductivity in contrast with the (100) SrTiO₃/LaAlO₃/Metal interfaces where t_c is smaller than the critical thickness for superconductivity. We attribute this dissimilarity to the different orbital polarization of e'_g for the (111) versus d_{xy} for the (001) interface.

Introduction

The interface between LaAlO₃ and SrTiO₃ exhibits two-dimensional conductivity¹, superconductivity², magnetism³⁻⁸, metal-insulator transition⁹, tunable Rashba spin-orbit interaction^{10,11}, quantum hall states^{12,13}, and one-dimensional conductivity^{14,15}. While the (100) SrTiO₃/LaAlO₃ interface received significant scientific attention, the (111) interface remains less explored.

Along the [111] direction in SrTiO₃ Ti forms triangular layers^{16,17}. Due to the trigonal symmetry the degeneracy of the t_{2g} manifold is lifted and they are further split into a_{1g} and e'_g orbitals. The six-fold symmetry of the titanium layer is reflected in the transport properties¹⁸. The symmetry is further reduced due to the structural transition of SrTiO₃ and the interface is predicted to host exotic superconductivity¹⁹, and topological states²⁰.

Four monolayers of LaAlO₃ are needed for the formation of a two-dimensional electron system (2DES) at the (100) SrTiO₃/LaAlO₃ interface⁹. For the (111) interface, the critical thickness for conductivity is nine monolayers (ML)¹⁶. The (111) 2DES also exhibits superconductivity²¹, with a link between superconductivity and spin-orbit interaction²². Notably, upon carrier depletion with negative gate voltage, superconductivity transitions into a Bose-insulating state²³. This behavior contrasts with the (100) interface where a weaker insulating state is observed for negative gate biases^{24,25}.

For spin injection and low voltage transistor applications, the barrier produced by the minimal four monolayers of LaAlO₃ required for conductivity at the bare (100) interface or by the nine monolayers at the (111) interface is relatively strong. Recent first principles calculations²⁶, and experimental studies of various metal capping on (100) interfaces (SrTiO₃/LaAlO₃/Metal)^{27,28} show that the critical thickness for the onset of conductivity, t_c , can be reduced relative to the bare interface and that t_c increases with the work function.

Here we study the problem of critical thickness for conductivity for (111) interfaces both experimentally and theoretically. We have also expanded our experimental research to the superconducting properties of both (100) and (111) SrTiO₃/LaAlO₃/metal interfaces. We find that upon capping the (111) SrTiO₃/LaAlO₃ interface with cobalt (Co) and platinum

(Pt), t_c is reduced from $t_c(\text{bare})=9$ ML to $t_c(\text{Co})=3$ ML and $t_c(\text{Pt})=6$ ML. Furthermore, once the (111) interface becomes conducting, it also becomes superconducting at low temperatures. This contrasts with the (100) interface where $t_c(\text{Pt})>t_c(\text{bare})$ and conductivity appears at t_c without superconductivity.

Concomitant density functional theory calculations with a Hubbard U term (DFT+ U) confirm the reduction of the critical thickness upon metal capping and indicate that conductivity at the (111) interface arises due to bands with e'_g orbital polarization. We conjecture that these bands are also responsible for superconductivity. This is in contrast with the (100) interface where the d_{xy} and the d_{yz}, d_{xz} bands are split due to their different effective masses along the direction of the confining potential (z -direction)²⁹. However, atomic spin-orbit interaction mixes them together³⁰. This new band-structure becomes non-rigid due to a Hubbard-type on-site repulsion with a lower-energy, non-superconducting band, and a higher-energy, mobile band, which is responsible to superconductivity^{17,31}.

Results

Experimental results

The transport measurements were performed on the samples with metal capping. In this configuration, the measured resistance is either a parallel combination of the metal cap resistance and the 2DES at the conducting SrTiO₃/LaAlO₃ interface or only the metallic cap in the absence of 2DES. We demonstrate this by measuring the transverse resistance R_{xy} , i.e., the Hall signal of the (111) SrTiO₃/LaAlO₃/Co/AlO_x interface for 4 LaAlO₃ ML, as shown in Fig.1. While for positive gate voltage, the 2DES dominates and exhibits signal resembling the (111) SrTiO₃/LaAlO₃ interface²² when depleting the 2DES by negative gate voltage, the contribution of Co predominates as manifested in an anomalous-Hall signal, confirming the presence of two parallel channels for conduction. This behavior is similar to (100) with cobalt capping²⁸.

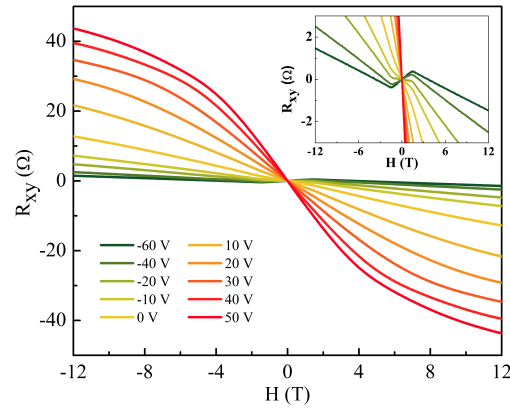


Figure 1. Transverse resistance of (111)SrTiO₃/LaAlO₃/Co/AlO_x for 4 ML LaAlO₃ as a function of a perpendicular magnetic field at different gate voltages. The inset focuses on the negative gate voltage regime. The observed anomalous-Hall signal demonstrates the predominance of the Co layer properties in this regime. This is in contrast to the higher carrier density regime where the 2DES dominates.

The transport studies conducted on (111) SrTiO₃/LaAlO₃/Co/AlO_x interface show a reduction of LaAlO₃ critical thickness for the onset of 2DES conductivity from 9 ML to 3 ML. In Fig.2 (a) we show the sheet resistance of (111)SrTiO₃/LaAlO₃/Co/AlO_x as a function of LaAlO₃ thickness at 40 K. For LaAlO₃ thickness below 3 ML, the resistance increases by nearly a factor of five. This indicates that 3 ML is the critical thickness of LaAlO₃ for the onset of conductivity with Co capping ($t_c(\text{Co})=3$ ML). To verify that a 2DES is formed parallel to the metallic layer, we measured the resistance versus back gate voltage. For a thin metallic layer parallel to a 2DES, one expects gate-dependent resistance due to the dominating contribution of 2DES. On the other hand, in the absence of a 2DES parallel to a metallic layer, we expect the gate dependence of the resistance to be immeasurably small due to the substantial carrier density in the metal. Fig. 2 (b) shows the gate dependence of (111) SrTiO₃/LaAlO₃/Co/AlO_x for 1 and 3 LaAlO₃ ML. For the sample with a single LaAlO₃ ML, the normalized resistance ($R/R_{(-60V)}$) is flat as a function of gate voltage, suggesting the absence of 2DES at the SrTiO₃/LaAlO₃ interface. For 3 ML LaAlO₃, the data show a significant gate dependence, suggesting the formation of a 2DES at (111)SrTiO₃/LaAlO₃ interface. We conclude that t_c becomes 3 ML upon Co capping for (111) interface.

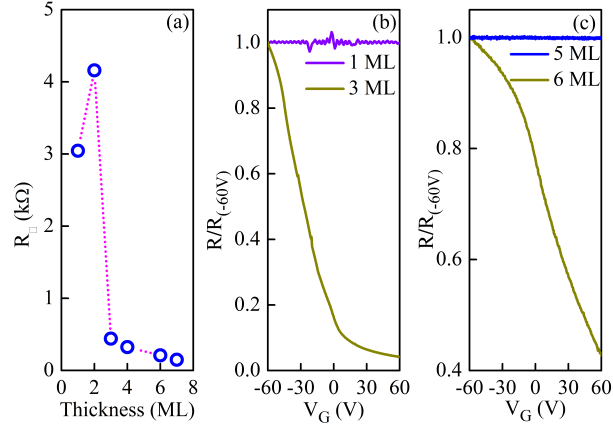


Figure 2. (a) The sheet resistance (R_{\square}) of (111) SrTiO₃/LaAlO₃/Co/AlO_x at 40 K as a function of LaAlO₃ thickness, an abrupt drop in the resistance at 3 ML indicates that this is the critical thickness for the formation of 2DES at the SrTiO₃/LaAlO₃ interface. Note: The measured samples were not patterned, the geometrical factor for the sheet resistance calculation is within an error bar of $\pm 10\%$. (b) The gate dependence of the normalized resistance ($R/R_{(-60V)}$) for (111) SrTiO₃/LaAlO₃/Co/AlO_x with LaAlO₃ thickness of 1 and 3 monolayers. (c) The gate dependence of normalized resistance ($R/R_{(-60V)}$) for (111) SrTiO₃/LaAlO₃/Pt for LaAlO₃ thickness of 5 and 6 monolayers.

Previous studies on the metal-capped (100) SrTiO₃/LaAlO₃ interface show that t_c increases with the work function of the metal-capping layer²⁶. To understand the role of the work function in (111) interfaces, we carried out experiments with Pt capping. The work function of platinum is generally higher than that of Co³². Surprisingly, we found that, unlike the (100) interface, Pt capping reduces the critical thickness from $t_c(\text{bare})=9$ ML to $t_c(\text{Pt})=6$ ML. This is demonstrated in Fig. 2(c), where we show the gate dependence of (111)SrTiO₃/LaAlO₃/Pt for 5 and 6 LaAlO₃ ML. The absence of gate dependence for 5ML and the strong gate dependence for 6ML suggests that $t_c(\text{Pt})=6$ ML. We interpret the saturation of the resistance at negative gate voltage as a result of depletion of the 2DES and dominance of the metal capping layer (see figure S2 in the supplementary information). In Figure S3 (Supplementary information), we also show the gate dependence of the extracted sheet resistance of 2DES for (111)SrTiO₃/LaAlO₃/Co/AlO_x and (111)SrTiO₃/LaAlO₃/Pt for 3 ML and 6 ML of LaAlO₃ respectively.

While suppression of t_c upon Co capping is observed for both the (111) and (100) SrTiO₃/LaAlO₃ interfaces, a reduction of t_c upon Pt capping is observed only for (111) interface, whereas an increase in t_c is found for the Pt capped (100) interface²⁸.

DFT results

In order to shed light on the origin of the experimentally observed critical thickness for an insulator-to-metal transition of the uncovered LaAlO₃ films on (111)SrTiO₃ as well as the role of metal capping, we have performed density functional theory calculations with a Hubbard U term. We considered different LaAlO₃ thicknesses and surface terminations, as well as metal capping using symmetric slabs with up to 130 atoms in the simulation cell. In the (111)-direction, the perovskite structure comprises a stacking of AO₃-B layers. Taking into account the formal charges in these compounds, this leads to alternating (SrO₃)⁴⁻ and Ti⁴⁺ layers in SrTiO₃ versus (LaO₃)³⁻ and Al³⁺ layers in LaAlO₃. In analogy to the (001) interface, one expects a Ti termination of (111)SrTiO₃, on top of which LaAlO₃ is deposited. However, for an integer number of LaAlO₃ layers, the resulting Al-termination resulted in an opposite internal electric field within LaAlO₃ than the one known from the (001)-oriented films³³⁻³⁵ with the valence band maximum in the top layer pushed to lower energies. This is, however, fully consistent with the charges of the stacked layers along the [111] direction. Moreover, the system is metallic as the bottom of the Ti 3d band touches the Fermi level, independent of the LaAlO₃ thickness, thus showing no indication for an insulator-to-metal transition with LaAlO₃ thickness in contrast with the experimental observation. Therefore, this configuration was discarded. We explored next a LaO₃ termination: While this generates an internal electric field with the correct sign with an upward shift of the valence band maximum in the LaAlO₃ layers as they approach the surface and a gradual reduction of the bandgap with increasing LaAlO₃ thickness, it generates holes in the surface LaO₃ layer. As a result, the Ti 3d band at the interface is pushed to higher energies, leading to a higher critical thickness than the one observed in the experiment. This indicates that some kind of compensation of the holes in the surface LaO₃ layer is necessary. To simulate this effect, we have tried different concentrations of hydrogen (H) in the surface layer and identified that a LaO₂(OH) termination with a single H on one out of three oxygens as displayed in Fig. 3 provides the correct charge to suppress the surface holes and to induce the

Effect of metal capping on superconducting properties

The DFT+ U calculations presented above unveil the origin of the critical thickness for a metal-to-insulator transition in (111)SrTiO₃/LaAlO₃ and the role of metal capping. We now turn to study the effect of metal capping on superconductivity for the (100) and (111) interfaces. Surprisingly, we find that all the (111) samples, which show conductivity upon metal capping, also show superconductivity. In table 2 and S1 (Supplemental information), we summarize the properties of the (100) and (111) interfaces with various LaAlO₃ thickness and different metal capping. Fig.6 displays the normalized resistance ($R/R_{(0.5K)}$) as a function of temperature for different (100) and (111) interfaces at the critical thickness t_c with Co and Pt capping.

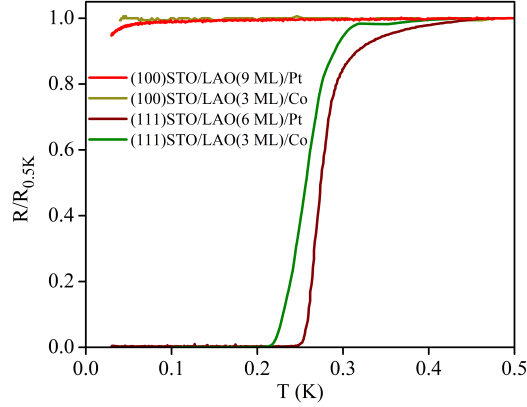


Figure 6. The normalized resistance ($R/R_{(0.5K)}$) of (100) SrTiO₃/LaAlO₃(3ML)/Co/AIO_x, (100)SrTiO₃/LaAlO₃(9ML)/Pt, (111) SrTiO₃/LaAlO₃(3ML)/ Co/AIO_x, and (111) SrTiO₃/LaAlO₃(6ML)/Pt. The LaAlO₃/SrTiO₃(111) interfaces capped with Co and Pt show a superconducting transition and the corresponding critical thickness of LaAlO₃ is 3 and 6 Monolayer respectively.

To make sure that the observed superconductivity is a two-dimensional (2D) interfacial effect and not a spurious one resulting from the metal deposition process, we studied the temperature dependence of the perpendicular and parallel critical field. We show in the supplementary information that they both follow the expected 2D Ginzburg-Landau temperature dependence (See Figure S4 of supplemental information).

In Fig.7 we show the behavior of the critical temperature and critical fields as a function of gate voltage for Co and Pt capped (111) interface. The dome-shaped gate dependence and the values of T_c , the perpendicular critical field H_{\perp} , and the parallel critical field H_{\parallel} are similar to the bare (111) SrTiO₃/LaAlO₃ interface^{17,22}.

One may claim that the absence of superconductivity in the Co-capped (100) SrTiO₃/LaAlO₃ is due to the Co ferromagnetism. Indeed, as shown previously in Fig.1, the Co layer shows an anomalous hall effect. However, for such a thin cobalt film, one expects the magnetic coupling to be short-ranged with a negligible effect on the 2DES. Nevertheless, to eliminate the possibility that the close proximity ($\sim 12\text{\AA}$) of the ferromagnetic Co to the interface is responsible for the absence of superconductivity in the (100) SrTiO₃/LaAlO₃/Co/AIO_x, we measured (non-magnetic) Ag capped (100) interface with 3 ML

Table 1. Calculated work functions (in eV) for different LaAlO₃ thicknesses (3, 6, and 9 ML), surface terminations (Al and LaO₃), partial surface hydrogenation [LaO₂(OH)], different metal cappings (Pt and Co), and of free-standing Pt(111) and Co(111) slabs of 7 ML thickness unstrained and strained to the lateral lattice constant of STO.

| | 3 ML | 6 ML | 9 ML |
|----------------------------|-----------------|-------|-------|
| Al | 4.478 | 4.599 | 4.534 |
| LaO ₃ | 5.153 | 5.042 | 5.146 |
| LaO ₂ (OH) | 4.186 | 4.193 | 4.631 |
| LaO ₃ /Pt | 6.080 | 6.076 | 6.072 |
| LaO ₃ /Co | 4.876 | 4.487 | |
| | Pt(111) Co(111) | | |
| Free-standing | 5.688 | 5.121 | |
| Strained@ a_{STO} | 5.734 | 4.780 | |

Table 2. Summary of the different samples measured for various thickness of LaAlO₃ upon different metal capping and corresponding nature of the interface. Note: For (100) interface one monolayer corresponds to one unit-cell (see also Table S1 (Supplemental information) for more samples).

| Interface | Metal layer | Thickness (ML) | Conducting | Super-Conducting |
|-----------|-------------|----------------|------------|------------------|
| (111) | Co | 2 | No | No |
| (111) | Co | 3 | Yes | Yes |
| (100) | Co | 2 | Yes | No |
| (100) | Co | 3 | Yes | No |
| (111) | Pt | 5 | No | No |
| (111) | Pt | 6 | Yes | Yes |
| (100) | Pt | 9 | Yes | No |
| (100) | Ag | 3 | Yes | No |

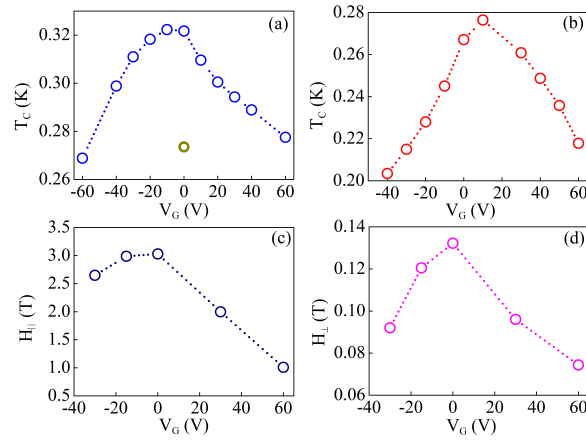


Figure 7. (a), The critical temperature (T_c) of (111) SrTiO₃/LaAlO₃(6ML)/Pt interface, the dark yellow circle shows the T_c of the as cooled film. (b), (c) and (d) are superconducting critical temperature, perpendicular critical field and parallel critical field respectively of the (111) SrTiO₃/LaAlO₃(3ML)/Co/AIO_x interface as a function of gate voltage. The values of these critical parameters are in good agreement with that of the uncapped interface. Note: T_c is defined as a temperature where the value of resistance drops by 50% of it's value at 0.5 K.

of LaAlO₃, which also shows no superconductivity, further demonstrating that the absence of superconductivity in capped (100) interfaces is not related to the ferromagnetism in the metal cap. In Figure S5 (Supplemental information), we show the temperature and gate bias dependence of the resistance for Ag capped (100) interface.

How can we understand the robustness of superconductivity in (111) interfaces? Previous experimental studies on (111) SrTiO₃/LaAlO₃ interfaces show that even at strong negative gate voltages, superconductivity remains intact^{22,23}. On the theory side, the curvature of the Fermi contour changes quickly upon charge accumulation, and both the conducting and superconducting bands get an equal contribution from the three degenerate t_{2g} orbitals¹⁷. By contrast, for (100) interface, there are distinct less mobile, non-superconducting band and a mobile superconducting band due to the very different effective masses of the light d_{xy} and heavy d_{yz} , d_{xz} bands. It is possible that the inter-band repulsion³¹ results in shifting the second band to higher energy leaving only the metallic state. Our DFT+ U calculations show that the e'_g bands are always present for the (111) conducting interfaces suggesting that this type of band plays a significant role in the observed superconductivity.

Methods

Epitaxial LaAlO₃ films with different thicknesses were grown on Ti, and TiO₂ terminated atomically smooth (111), and (100) SrTiO₃ substrates respectively at an oxygen pressure of 1×10^{-4} Torr and temperature 780°C using pulsed laser deposition. The thickness was in-situ monitored by reflection high energy electron diffraction (RHEED) (see supplementary information Figure S1). The samples were then transferred to a metal deposition chamber (e-beam for the Co and Ag and Sputtering or

e-beam for the Pt) where they were pre-annealed for two minutes at 200°C and at a pressure of 1×10^{-8} Torr to remove surface contaminants. Metallic layers of ≈ 3 nm of platinum (Pt), silver (Ag), or cobalt (Co) were deposited at room temperature. For the latter, we used an additional 3 nm AlO_x to prevent oxidation. Wire bonding was used to connect to the sample electrically. Density functional theory (DFT) calculations were performed on thin LaAlO_3 films on (111)-oriented SrTiO_3 , using the projector augmented wave (PAW) method³⁸ as implemented in the VASP code³⁹. The generalized gradient approximation was used for the exchange-correlation functional, as parametrized by Perdew, Burke, and Ernzerhof⁴⁰. Static correlation effects were considered within the DFT+ U formalism⁴¹, employing $U = 3$ eV for the Ti 3d orbitals, in line with previous work^{42–44}. The LaAlO_3 thin films on (111) SrTiO_3 were modeled in the slab geometry with two symmetric surfaces to eliminate spurious electric fields. The (111) $\text{SrTiO}_3/\text{LaAlO}_3$ slabs contain 7 monolayers (ML) of SrTiO_3 (substrate) and 3–9 ML of LaAlO_3 on both sides of the substrate. Additionally, in order to assess the role of metallic contacts, a Pt and Co ML was added on top of the LaAlO_3 film. The modeled slabs contain ~ 60 atoms for 3 ML LaAlO_3 and ~ 120 atoms for 9 ML LaAlO_3 , depending on surface termination and metal capping. The lateral lattice constant of the modeled (111) $\text{SrTiO}_3/\text{LaAlO}_3$ slabs was fixed to the SrTiO_3 substrate ($\sqrt{2}a \times \sqrt{2}a$ lateral unit cell with $a = 3.905$ Å). A vacuum region of 15 Å was adopted to minimize the interaction between the slab and its periodic images. A cutoff energy of 600 eV was used to truncate the plane-wave expansion and a Γ -centered k -point mesh of $12 \times 12 \times 1$ to sample the Brillouin zone (BZ). The atomic positions were fully optimized taking into account octahedral rotations and distortions until the forces on all atoms were less than 0.01 eV/Å and the change in total energy was less than 10^{-6} eV. Spin polarization was also considered in the DFT+ U calculations to account for possible magnetic moments of the Ti 3d electrons and the metal capping layer.

References

- Ohtomo, A. & Hwang, H. Y. *Nature* **427**, 423 (2004).
- Reyren, N. *et al. Science* **317**, 1196 (2007).
- Brinkman, A. *et al. Nat. Mater.* **6**, 493 (2007).
- Sachs, M. *et al. Anomalous magneto-transport at the superconducting interface between LaAlO_3 and SrTiO_3 . Phys. C: Supercond. its applications* **470**, S746–S748 (2010).
- Bert, J. A. *et al. Nat. Phys.* **7**, 767 (2011).
- Ron, A., Maniv, E., Graf, D., Park, J.-H. & Dagan, Y. *Phys. Rev. Lett.* **113**, 216801 (2014).
- Seri, S. & Klein, L. *Phys. Rev. B* **80**, 180410 (2009).
- Lee, J.-S. *et al. Titanium d xy ferromagnetism at the $\text{LaAlO}_3/\text{SrTiO}_3$ interface. Nat. Mater.* **12**, 703–706 (2013).
- Thiel, S., Hammerl, G., Schmehl, A., Schneider, C. W. & Mannhart, J. Tunable quasi-two-dimensional electron gases in oxide heterostructures. *Science* **313**, 1942–1945 (2006).
- Ben Shalom, M., Sachs, M., Rakhmilevitch, D., Palevski, A. & Dagan, Y. *Phys. Rev. Lett.* **104**, 126802 (2010).
- Caviglia, A. *et al. Tunable Rashba spin-orbit interaction at oxide interfaces. Phys. Rev. Lett.* **104**, 126803 (2010).
- Xie, Y. *et al. Quantum longitudinal and Hall transport at the $\text{LaAlO}_3/\text{SrTiO}_3$ interface at low electron densities. Solid state communications* **197**, 25–29 (2014).
- Trier, F. *et al. Quantization of Hall resistance at the metallic interface between an oxide insulator and SrTiO_3 . Phys. Rev. Lett.* **117**, 096804 (2016).
- Ron, A. & Dagan, Y. One-dimensional quantum wire formed at the boundary between two insulating $\text{LaAlO}_3/\text{SrTiO}_3$ interfaces. *Phys. Rev. Lett.* **112**, 136801 (2014).
- Briggeman, M. *et al. Pascal conductance series in ballistic one-dimensional $\text{LaAlO}_3/\text{SrTiO}_3$ channels. Science* **367**, 769–772 (2020).
- Herranz, G., Sánchez, F., Dix, N., Scigaj, M. & Fontcuberta, J. *Sci. Rep.* **2**, 758 (2012).
- Khanna, U. *et al. Symmetry and correlation effects on band structure explain the anomalous transport properties of (111) $\text{LaAlO}_3/\text{SrTiO}_3$. Phys. Rev. Lett.* **123**, 036805 (2019).
- Rout, P. K., Agireen, I., Maniv, E., Goldstein, M. & Dagan, Y. *Phys. Rev. B* **95**, 241107 (2017).
- Hecker, M. & Schmalian, J. Vestigial nematic order and superconductivity in the doped topological insulator $\text{Cu}_x\text{Bi}_2\text{Se}_3$. *npj Quantum Mater.* **3**, 1–6 (2018).
- Doennig, D., Pickett, W. E. & Pentcheva, R. *Phys. Rev. Lett.* **111**, 126804 (2013).

21. Monteiro, A. M. R. V. L. *et al.* Two-dimensional superconductivity at the (111)LaAlO₃/SrTiO₃ interface. *Phys. Rev. B* **96**, 020504, DOI: [10.1103/PhysRevB.96.020504](https://doi.org/10.1103/PhysRevB.96.020504) (2017).
22. Rout, P. K., Maniv, E. & Dagan, Y. Link between the superconducting dome and spin-orbit interaction in the (111)LaAlO₃/SrTiO₃ interface. *Phys. Rev. Lett.* **119**, 237002, DOI: [10.1103/PhysRevLett.119.237002](https://doi.org/10.1103/PhysRevLett.119.237002) (2017).
23. Mograbi, M. *et al.* Vortex excitations in the insulating state of an oxide interface. *Phys. Rev. B* **99**, 094507, DOI: [10.1103/PhysRevB.99.094507](https://doi.org/10.1103/PhysRevB.99.094507) (2019).
24. Caviglia, A. D. *et al.* *Nature* **456**, 624 (2008).
25. Chen, Z. *et al.* Carrier density and disorder tuned superconductor-metal transition in a two-dimensional electron system. *Nat. communications* **9**, 1–6 (2018).
26. Arras, R., Ruiz, V. G., Pickett, W. E. & Pentcheva, R. Tuning the two-dimensional electron gas at the LaAlO₃/SrTiO₃(001) interface by metallic contacts. *Phys. Rev. B* **85**, 125404, DOI: [10.1103/PhysRevB.85.125404](https://doi.org/10.1103/PhysRevB.85.125404) (2012).
27. Lesne, E. *et al.* *Nat. Commun.* **5** (2014).
28. Vaz, D. C. *et al.* Tuning up or down the critical thickness in LaAlO₃/SrTiO₃ through in situ deposition of metal overlayers. *Adv. Mater.* **29**, 1700486, DOI: [10.1002/adma.201700486](https://doi.org/10.1002/adma.201700486) (2017).
29. Santander-Syro, A. F. *et al.* *Nature* **2011**, 189 (2011).
30. Joshua, A., Pecker, S., Ruhman, J., Altman, E. & Ilani, S. *Nat. Commun.* **3**, 1129 (2012).
31. Maniv, E. *et al.* *Nat. Commun.* **6**, 8239 (2015).
32. Michaelson, H. B. *J. Appl. Phys.* **48**, 4729 (1977).
33. Pentcheva, R. & Pickett, W. E. Avoiding the Polarization Catastrophe in LaAlO_3 Overlayers on SrTiO_3 (001) through Polar Distortion. *Phys. Rev. Lett.* **102**, 107602, DOI: [10.1103/PhysRevLett.102.107602](https://doi.org/10.1103/PhysRevLett.102.107602) (2009).
34. Pentcheva, R. *et al.* Parallel Electron-Hole Bilayer Conductivity from Electronic Interface Reconstruction. *Phys. Rev. Lett.* **104**, 166804, DOI: [10.1103/PhysRevLett.104.166804](https://doi.org/10.1103/PhysRevLett.104.166804) (2010).
35. Singh-Bhalla, G. *et al.* Unexpected termination switching and polarity compensation in LaAlO₃/SrTiO₃ heterostructures. *Phys. Rev. Mater.* **2**, 112001, DOI: [10.1103/PhysRevMaterials.2.112001](https://doi.org/10.1103/PhysRevMaterials.2.112001) (2018).
36. Yu, L. & Zunger, A. A polarity-induced defect mechanism for conductivity and magnetism at polar–nonpolar oxide interfaces. *Nat. Commun.* **5**, 5118, DOI: [10.1038/ncomms6118](https://doi.org/10.1038/ncomms6118) (2014).
37. Min, T. *et al.* Cooperative evolution of polar distortion and nonpolar rotation of oxygen octahedra in oxide heterostructures. *Sci. Adv.* **7**, eabe9053 (2021).
38. Kresse, G. & Joubert, D. From ultrasoft pseudopotentials to the projector augmented-wave method. *Phys. Rev. B* **59**, 1758–1775, DOI: [10.1103/PhysRevB.59.1758](https://doi.org/10.1103/PhysRevB.59.1758) (1999).
39. Kresse, G. & Furthmüller, J. Efficient iterative schemes for ab initio total-energy calculations using a plane-wave basis set. *Phys. Rev. B* **54**, 11169–11186, DOI: [10.1103/PhysRevB.54.11169](https://doi.org/10.1103/PhysRevB.54.11169) (1996).
40. Perdew, J. P., Burke, K. & Ernzerhof, M. Generalized Gradient Approximation Made Simple. *Phys. Rev. Lett.* **77**, 3865–3868, DOI: [10.1103/PhysRevLett.77.3865](https://doi.org/10.1103/PhysRevLett.77.3865) (1996).
41. Dudarev, S. L., Botton, G. A., Savrasov, S. Y., Humphreys, C. J. & Sutton, A. P. Electron-energy-loss spectra and the structural stability of nickel oxide: An LSDA+U study. *Phys. Rev. B* **57**, 1505–1509, DOI: [10.1103/PhysRevB.57.1505](https://doi.org/10.1103/PhysRevB.57.1505) (1998).
42. Nolan, M. *et al.* Electronic structure of point defects in controlled self-doping of the TiO_2 (110) surface: Combined photoemission spectroscopy and density functional theory study. *Phys. Rev. B* **77**, 235424, DOI: [10.1103/PhysRevB.77.235424](https://doi.org/10.1103/PhysRevB.77.235424) (2008).
43. Betancourt, J., Paudel, T. R., Tsymbal, E. Y. & Velez, J. P. Spin-polarized two-dimensional electron gas at $\text{GdTiO}_3/\text{SrTiO}_3$ interfaces: Insight from first-principles calculations. *Phys. Rev. B* **96**, 045113, DOI: [10.1103/PhysRevB.96.045113](https://doi.org/10.1103/PhysRevB.96.045113) (2017).
44. Geisler, B., Blanca-Romero, A. & Pentcheva, R. Design of n- and p-type oxide thermoelectrics in $\text{LaNiO}_3/\text{SrTiO}_3$ (001) superlattices exploiting interface polarity. *Phys. Rev. B* **95**, 125301, DOI: [10.1103/PhysRevB.95.125301](https://doi.org/10.1103/PhysRevB.95.125301) (2017).

Acknowledgements

We thank Moshe Goldstein and Udit Khanna for useful discussions. This research was supported by the Bi-national Science Foundation under grant 2014047 and by the Israel Science Foundation under grant : 382/17. RP and LL acknowledge computational time at the Leibniz Rechenzentrum, project pr87ro.

Author contributions statement

Y.D., A.G.S., and H.Y.H conceived the experiment. R.S.B., M.M.,and P.K.R. made the samples. H.Y, A.G.S. and R.S.B. did the metallization. R.S.B., M.M., P.K.R., and G.T. conducted the transport measurements and analyzed the data. R. P. conceived the theoretical modelling and L.L.L. performed the DFT calculations. R.S.B., L.L.L, R.P., and Y.D. wrote the paper. All authors reviewed the manuscript.

Supplementary information for Concomitant appearance of conductivity and superconductivity in (111) LaAlO₃/SrTiO₃ interface with metal capping

S1: Reflection-high energy electron diffraction (RHEED) oscillations for LaAlO₃ film grown on SrTiO₃ (111) and (100) substrates respectively

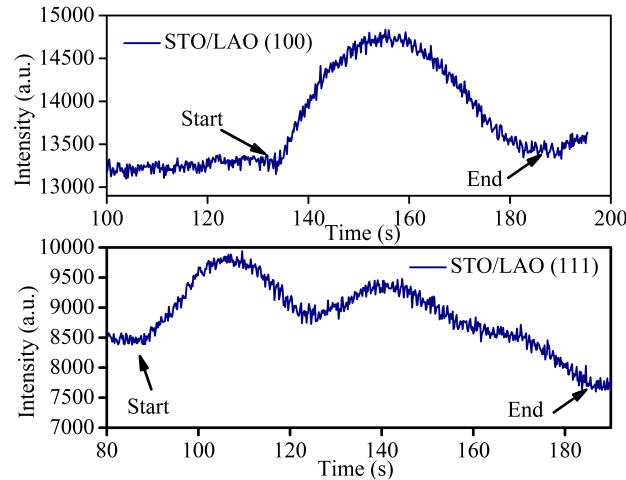


Figure 8. S1 : Reflection-high energy electron diffraction (RHEED) oscillations monitored during the deposition of LaAlO₃ on SrTiO₃ (111) and (100) substrate suggests a layer by layer growth of the film. Each oscillation corresponds to the one monolayer.

S2: Normalized resistance ($R/R_{(-400V)}$) of (111) SrTiO₃/LaAlO₃(6ML)/Pt

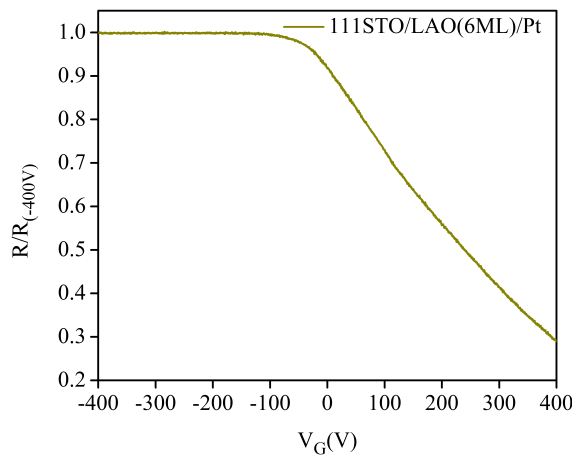


Figure 9. S2 : The normalized resistance ($R/R_{(-400V)}$) of (111) SrTiO₃/LaAlO₃(6ML)/Pt sample suggests a complete depletion of 2DES at negative gate voltages and a dominating contribution of metal overlayer.

S3: Sheet Resistance of two dimensional electron system without Capping

The sheet resistance of the two dimensional electron system (2DES) without capping was extracted from the analysis of the parallel resistance model as given in the equation 1. Where $R_{Measured}$, $R_{Metal-Overlayer}$, and R_{2DES} is the experimentally

measured resistance of the parallel conducting channel, resistance of metal overlayer, and resistance of the 2DES respectively. In our analysis we assumed $R_{metal-capping} = R_{Measured}$ at strong negative gate voltages. Figure S3 represents the extracted sheet resistance of the 2DES for (111)SrTiO₃/LaAlO₃/Co/AIO_x and (111)SrTiO₃/LaAlO₃/Pt samples for 3 and 6 ML LaAlO₃ as a function of gate voltages. The diverging nature of the resistance at negative gate voltage is expected for a depleted 2DES.

$$\frac{1}{R_{Measured}} = \frac{1}{R_{Metal-Overlayer}} + \frac{1}{R_{2DES}} \quad (1)$$

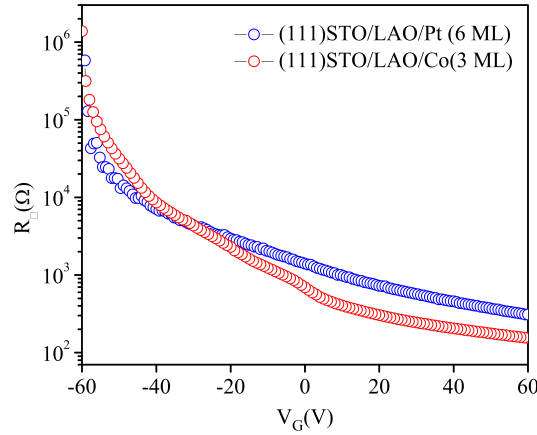


Figure 10. S3 : The extracted sheet resistance of (111)SrTiO₃/LaAlO₃/Co/AIO_x and (111)SrTiO₃/LaAlO₃/Pt samples for 3 and 6 ML of LaAlO₃ as a function of a gate voltages. The resistance was extracted according to the equation 1. A diverging nature of the resistance at negative gate represents the depletion of the 2DES.

Table S1: The extension of table 1 from the main text. Summary of the different samples measured for various thickness of LaAlO₃ upon different metal capping and corresponding nature of the interface.

| Interface | Metal layer | Thickness (ML) | Conducting | Super-Conducting |
|-----------|-------------|----------------|------------|------------------|
| (111) | Co | 1 | No | No |
| (111) | Co | 2 | No | No |
| (111) | Co | 3 | Yes | Yes |
| (111) | Co | 4 | Yes | Yes |
| (111) | Co | 6 | Yes | Yes |
| (111) | Co | 7 | Yes | Yes |
| (111) | Pt | 5 | No | No |
| (111) | Pt | 6 | Yes | Yes |
| (111) | Pt | 9 | Yes | Yes |
| (111) | Pt | 12 | Yes | Yes |
| (100) | Co | 2 | Yes | No |
| (100) | Co | 3 | Yes | No |
| (100) | Pt | 9 | Yes | No |
| (100) | Ag | 3 | Yes | No |

S4: Analysis of critical fields

Temperature dependence of perpendicular and parallel critical fields were analyzed according to the phenomenological Ginzburg-landau theory for the 2-dimensional nature of the superconductivity. The perpendicular and parallel critical fields in the framework of the Ginzburg-landau theory follow equation 2 and 3 respectively. In Figure S4, we show the fit to equation 2 and 3 for (111)SrTiO₃/LaAlO₃(3ML)/Co interface. The extracted perpendicular (H_{\perp}) and parallel critical field (H_{\parallel}) as a

fuction of gate voltages has been shown in Figure 7 of the main text.

$$H_{\perp} = \frac{\phi_0}{2\pi\xi^2} \left(1 - \frac{T}{T_c}\right) \quad (2)$$

$$H_{\parallel} = \frac{\phi_0\sqrt{12}}{2\pi\xi^2d} \left(1 - \frac{T}{T_c}\right)^{\frac{1}{2}} \quad (3)$$

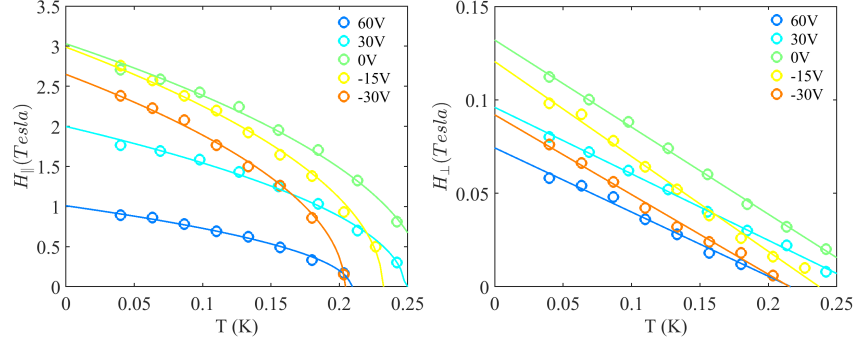


Figure 11. S4: The perpendicular (H_{\perp}) and parallel critical field (H_{\parallel}) as a fuction of temperature for (111)SrTiO₃/LaAlO₃(3ML)/Co interface. The solid lines are fit to the equation 2 and 3.

S5: Role of Ag Capping

To show that absence of superconductivity in co-capped (100) SrTiO₃/LaAlO₃ interface is not related to ferromagnetism in the cobalt, we used silver (Ag) capping. Ag has low work function and can therefore reduce the critical thickness by increasing the charge transfer. The measured Ag capped (100) interface for 3 monolayers (ML) of LaAlO₃ does not show full superconducting transition for any gate voltage. This confirms that ferromagnetism of Co is not the cause for the absence of superconductivity in (100) co-capped interfaces. In Figure S5 we show the sheet resistance of Ag capped (100)SrTiO₃/LaAlO₃ as a function of temperature at different positive gate voltages. A dip in the sheet resistance can be attributed due to the localized superconducting regions which are not connected percolatively even on application of positive gate bias. These localized regions may arise from a slight thickness nonuniformity. The data thus suggest there is no macroscopic superconductivity present in (100)SrTiO₃/LaAlO₃ interface below the bare critical thickness upon metal capping.

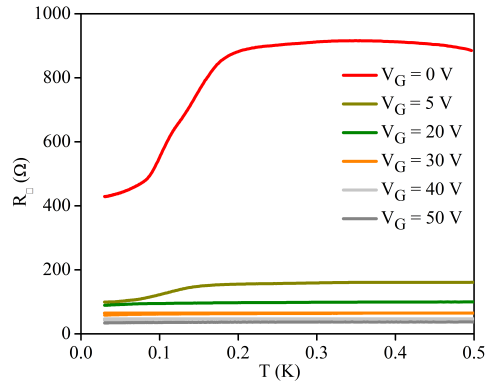


Figure 12. S5: The sheet resistance of (100) SrTiO₃/ LaAlO₃/Ag interface for 3 LaAlO₃ ML as a function of temperature at different gate voltages shows an absence of superconductivity. A dip in the resistance can be attributed to the localized superconducting regions which may result from a thickness inhomogeneity of LaAlO₃ .